13th International Symposium on Turbulence and Shear Flow Phenomena (TSFP13)
Montreal, Canada, June 25–28, 2024

REDUCING JET NOISE FROM AN UNDEREXPANDED BICONICAL NOZZLE

Daniel J. Bodony
Department of Aerospace Engineering
University of Illinois at Urbana-Champaign
Urbana, IL, 61801, USA
bodony@illinois.edu

Sandeep Murthy
Department of Aerospace Engineering
University of Illinois at Urbana-Champaign
Urbana, IL, 61801, USA
srmurth2@illinois.edu

ABSTRACT

The intense noise radiated by jet aircraft exhaust nozzles causes structural vibration, fatigue, carrier deck personnel operational difficulties, and community environmental concerns. Prior work into the physics and control of jet noise have identified several important sound sources, including wavepackets, screech, Mach wave radiation, and broadband shock associated noise, to name a few. Reducing the loudest sources of jet noise, without sacrificing propulsive performance, has thus-far relied on intuition, parametric survey, or optimal control techniques. With the aim of developing a more general and robust method of jet noise reduction (JNR), we seek a physics-based JNR approach that is built upon a linear resolvent analysis appropriate for mean flows with strong shocks. The effect of flow discontinuities on the underlying linear analysis, including the optimal forcing and response modes that arise from resolvents, is also investigated.

BACKGROUND

High speed jet noise from Naval tactical aircraft causes operational difficulties limiting communication between pilot and carrier deck crew, quickly damages deck crew hearing, and leads to sound-induced structural vibrations and fatigue. Several decades of experimental, theoretical, and computational investigations into the physics and control of jet noise have identified several important sound sources, including wavepackets (Jordan & Colonius, 2013), screech (Ponton & Seiner, 1992), Mach wave radiation (Williams & Maidanik, 1965), and broadband shock associated noise (Norum & Seiner, 1982). Reducing the loudest sources of jet noise, without sacrificing propulsive performance, has relied on intuition (Seiner *et al.*, 2004), parametric survey (Bridges & Brown, 2004), or optimal control techniques (Kim *et al.*, 2014).

A promising framework to understand aerodynamic turbulent jet noise is formulated by constructing a linearised Navier-Stokes system subject to stochastic forcing such that the statistical moments of the turbulent flow are governed by model equations (Farrell & Ioannou, 1993, 2019). Literature that investigates such a stochastic forcing applied to linearised Navier-Stokes equations predominantly focus on time-domain formulations of covariance dynamics; however, coherence in jet turbulence has often been analyzed in the frequency domain (Lesshafft *et al.*, 2019). Spectral proper orthogonal decomposition (SPOD) has been used as a means to extract empirical coherent structures at a given frequency from numerical flow data (Garnaud *et al.*, 2013; Lesshafft *et al.*, 2019; Gudmundsson & Colonius, 2011). Recently, linear stability analyses of jets have been carried out in a frequency-domain framework using optimal forcing/response structures (Garnaud *et al.*, 2013). The forcing and response modes in this formalism are global in nature, and they are constructed as the singular modes of the global resolvent operator (Schmid, 2007). This analysis has been employed to model the stochastic dynamics of the Navier-Stokes equations (Sipp & Marquet, 2013). The work by Beneddine *et al.* (2016) demonstrates that the spatial structure of the optimal linear flow response agree with the leading SPOD modes, obtained from numerical simulations, and has established a formal justification for a direct comparison between optimal linear response structures and SPOD modes.

This paper describes current research towards extending linear-based JNR strategies to jets with strong shocks. Although such jets are common in high-performance aircraft, there is scant literature discussing forward and adjoint sensitivity analyses about flows with discontinuities in general, with even less prior work within the computational fluid dynamics realm. The question of how to address sensitivities with shock-laden flows follows a presentation of our large-eddy simulation framework applied to underexpanded jets.

LARGE EDDY SIMULATION RESULTS

Using an optimized WENO-based shock capturing scheme, with a Ducros shock sensor, the shock-laden turbulent flow issuing from a biconical nozzle (figure 1) with nozzle pressure ratio (NPR = $p_0/p_\infty = 4$) have been simulated for a series three total temperature ratios (TTR = $T_0/T_\infty = 1,3,7$), using a specific heat ratio of $\gamma = 1.4$, a Prandtl number of $\mathrm{Pr} = 0.72$, and a dynamic LES model (Moin *et al.*, 1991). The flow fields corresponding to the TTR = 1 conditions are shown, along with their corresponding sound fields, in the following figures (figures 2–4). Results from the higher temperature jets are available in Murthy & Bodony (2023). For TTR = 1, the LES predictions faithfully match the experimental data along the jet centerline and away from it. The flow is characterized by a strong shock cell pattern near the nozzle exit that initiates with a normal shock. More detailed analysis of the jet and near-jet fields are provided in Murthy & Bodony (2023).

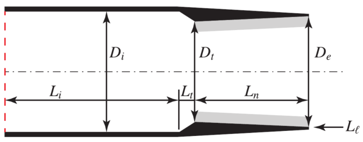

Parameter	Value
D_t/D_e	67.06/72.85
L_t/D_e	9.75/72.85
L_n/D_e	73.56/72.85
D_i/D_e	79.34/72.85
L_i/D_e	1.09
L_ℓ/D_e	0.508/72.85

Figure 1. Biconical nozzle geometric parameters.

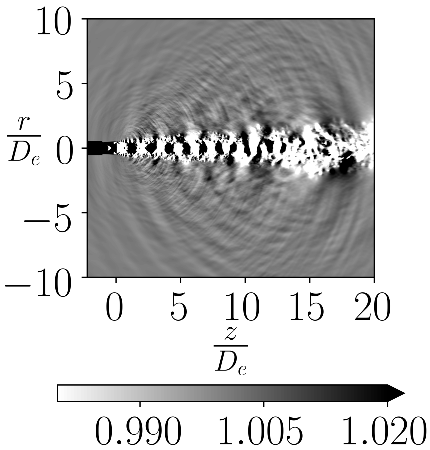

Figure 2. Instantaneous pressure field for NPR = 4, TTR = 1 jet.

JET NOISE REDUCTION USING LINEARIZED ANALYSIS OF THE MEAN FLOW

A linear analysis about the jet mean flow to support JNR is performed. The presence of the strong shocks in the jet mean flow, particularly the "barrel shock" that forms along the centerline just downstream of the nozzle exit, implies that care must be taken when considering the linearized dynamics, especially when the linearized operator depends on the smooth definition of the derivative. We analyzed the impact of shocks on linearized operator construction in Bodony & Fikl (2022).

We view JNR as modifications to the linearized, discretized flow equations,

$$\frac{\mathrm{d}\boldsymbol{Q}'}{\mathrm{d}t} = \boldsymbol{L}(\bar{\boldsymbol{Q}})\,\boldsymbol{Q}' + \boldsymbol{B}\,\boldsymbol{f}, \quad \boldsymbol{r} = \boldsymbol{C}\,\boldsymbol{Q}', \tag{1}$$

where the vector $\boldsymbol{f}$ contains zero-mean source terms of the continuity, momentum and energy equations, and represents an external forcing on the linearized-compressible-Navier-Stokes equations. The vector $\boldsymbol{r}$ represents the vector holding the quantity of interest, that is, the far-field pressure fluctuations. The matrices $\boldsymbol{B}$ and $\boldsymbol{C}$ specify the inputs—to (turbulent kinetic energy fluctuations) and outputs—from (far-field pressure fluctuations) the resolvent analysis that help reveal the influence of the jet on the far-field acoustics.

Defining the norm used to measure the input and output mode energy as shown below

$$||\hat{\boldsymbol{r}}||^2 = \hat{\boldsymbol{r}}^H\,\boldsymbol{D}_r\,\hat{\boldsymbol{r}} = \hat{\boldsymbol{r}}^H\,\boldsymbol{N}_r^H\,\boldsymbol{N}_r\,\hat{\boldsymbol{r}}, \tag{2}$$

$$||\hat{\boldsymbol{f}}||^2 = \hat{\boldsymbol{f}}^H\,\boldsymbol{D}_f\,\hat{\boldsymbol{f}} = \hat{\boldsymbol{f}}^H\,\boldsymbol{N}_f^H\,\boldsymbol{N}_f\,\hat{\boldsymbol{f}}, \tag{3}$$

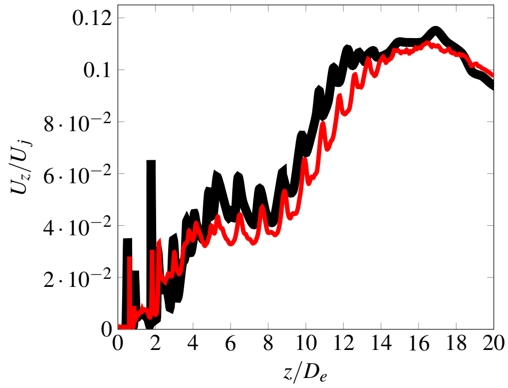

Figure 3. TTR = 1, NPR = 4, LES-based centerline axial turbulence intensity (red line) comparison against LES simulation data (black line) from Liu & Corrigan (2018).

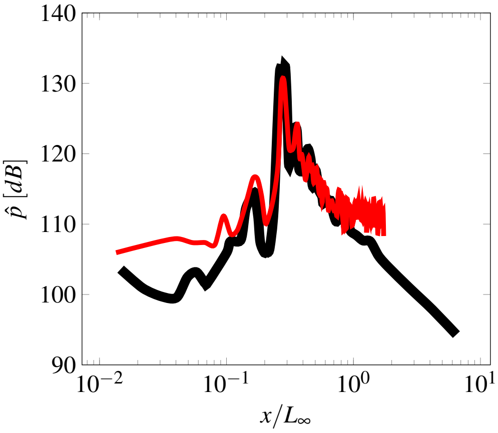

Figure 4. TTR = 1, NPR = 4, LES-based SPL calculation at $(z/D_e, r/D_e) = (0, 1.5)$ (red line) compared against experimental data (black line) from Liu *et al.* (2013).

an expression for the gain between input and output energy is

$$\sigma^2 = \frac{||\hat{\boldsymbol{r}}||^2}{||\hat{\boldsymbol{f}}||^2} = \frac{\hat{\boldsymbol{f}}^H\,\boldsymbol{H}^H(\omega)\,\boldsymbol{N}_r^H\,\boldsymbol{N}_r\,\boldsymbol{H}(\omega)\,\hat{\boldsymbol{f}}}{\hat{\boldsymbol{f}}^H\,\boldsymbol{N}_f^H\,\boldsymbol{N}_f\,\hat{\boldsymbol{f}}}. \tag{4}$$

The expression for gain in Eq. (4) can be viewed as a Rayleigh quotient, involving the Hermitian operator $\boldsymbol{N}_f^{-H}\,\boldsymbol{H}^H(\omega)\,\boldsymbol{N}_r^H\boldsymbol{N}_r\,\boldsymbol{H}(\omega)\,\boldsymbol{N}_f^{-1}$. In other words, σ is equal to the largest singluar value of the operator $\boldsymbol{N}_r\,\boldsymbol{H}(\omega)\,\boldsymbol{N}_f^{-1} = \boldsymbol{U}\boldsymbol{\Sigma}\boldsymbol{V}^H$ and the forcing and response structures that feature the largest gains are given by $\hat{\boldsymbol{f}}_{\boldsymbol{i}} = \boldsymbol{N}_{\boldsymbol{f}}^{-1}\hat{\boldsymbol{v}}_{\boldsymbol{i}}$ ($\hat{\boldsymbol{v}}_{\boldsymbol{i}}$ are columns of $\boldsymbol{V}$) and $\hat{\boldsymbol{r}}_{\boldsymbol{i}} = \sigma_i \boldsymbol{N}_{\boldsymbol{r}}^{-1}\hat{\boldsymbol{u}}_{\boldsymbol{i}}$ ($\hat{\boldsymbol{u}}_{\boldsymbol{i}}$ are columns of $\boldsymbol{U}$ and σ_i are the corresponding singular values), respectively.

By the hypothesis that JNR is accompanied by a reduction in the gain as defined above, a discrete structural sensitivity analysis gives an estimate of the change in gain (dσ), due to the linear feedback control of $\boldsymbol{f} = \alpha\boldsymbol{C}\boldsymbol{Q}'$, for values of α that would allow the matrix $\alpha\boldsymbol{C}$ to be viewed as a perturbation $\boldsymbol{dL}$ to the operator $\boldsymbol{L}(\bar{\boldsymbol{Q}})$ in the linear limit as

$$\mathrm{d}\sigma \approx \mathrm{Re}\left(\hat{\boldsymbol{u}}^H(\boldsymbol{N}_r\boldsymbol{C}\,(\boldsymbol{R}\,\boldsymbol{dL}\,\boldsymbol{R})\,\boldsymbol{B}\boldsymbol{N}_f^{-1})\,\hat{\boldsymbol{v}}/(\hat{\boldsymbol{u}}^H\hat{\boldsymbol{u}})\right). \tag{5}$$

The JNR objective is to optimize the movement of the chosen target singular value. The optimization seeks, for the case of

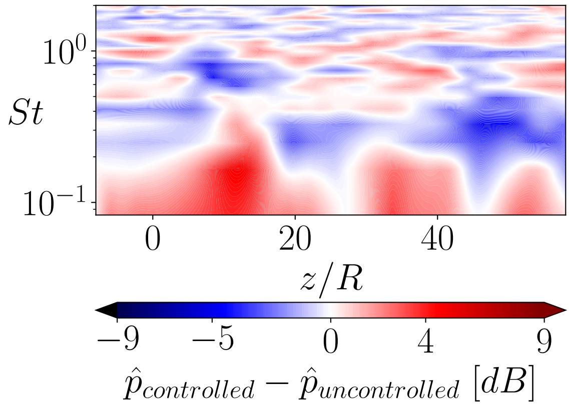

Figure 5. TTR = 1, NPR = 4, SPL contour plot corresponding to the un-controlled (top left), controlled (top right) and difference between the un-controlled and controlled (bottom) over the region defined by $r/R = 20$ and $z/R \in [-8, 58]$.

gain (σ) minimization, the solution $\boldsymbol{C}^* \equiv \mathrm{Re}\left(\alpha^{-1}\mathrm{d}\sigma\right)$, with respect to the parameters $\left\{\tilde{\boldsymbol{C}}, x_0, y_0, z_0, \ell_x, \ell_y, \ell_z\right\}$ and over the field of $\boldsymbol{C}$ of unit norm.

Upon performing the optimization for a target frequency $St = 0.3$ and implementing the subsequent parameters into the original LES calculation, the change in the SPL on a cylindrical surface is shown in figure 5. The figure clearly shows an overall reduction for frequencies near $St = 0.3$, but also some residual increases elsewhere.

CONVERGENT RESOLVENT MODE CALCULATIONS IN SHOCK-LADEN FLOWS

The resolvent analysis of the previous section is now reexamined with focus placed on the shock and its impact on the forward and adjoint sensitivities, and the resolvent. We start with the zero-frequency resolvent analysis of inviscid shock-laden quasi-1d flows presented in Murthy & Bodony (2023) with the goal to understand why resolvent modes corresponding to inviscid shock-laden flows may not agree with numerical solutions that feature shock capturing (Bodony & Fikl, 2022). Our approach will be to extend the analysis of Giles & Pierce (2001) to include viscosity and examine the operators in the limit of vanishing viscosity.

Viscous flow equations: We consider the viscous quasi-1d equations,

$$\vec{R}(\vec{U},h) = \frac{d}{dx}(h\vec{F}) + \frac{d}{dx}\left(h\frac{d}{dx}(\vec{F}_{v,1})\right) + \frac{dh}{dx}\frac{d}{dx}(\vec{F}_{v,2}) - \frac{dh}{dx}\vec{P} = \vec{0}, \tag{6}$$

where $\vec{U} = \begin{bmatrix}\rho \\ \rho q \\ \rho E\end{bmatrix}$, $\vec{F} = \begin{bmatrix}\rho q \\ \rho q^2 + p \\ \rho q H\end{bmatrix}$, $\vec{F}_{v,1} = \begin{bmatrix}0 \\ -\frac{4\mu q}{3} \\ -\frac{2\mu q^2}{3} - \frac{c_p \mu T}{Pr}\end{bmatrix}$, $\vec{F}_{v,2} = \begin{bmatrix}0 \\ \frac{4\mu q}{3} \\ 0\end{bmatrix}$, $\vec{P} = \begin{bmatrix}0 \\ p \\ 0\end{bmatrix}$ and $H = E + \frac{p}{\rho} = \frac{\gamma}{\gamma-1}\frac{p}{\rho} + \frac{1}{2}q^2$.

Viscous linear forward operator and basis solutions: Starting with these viscous quasi-1d non-linear equations, the corresponding viscous linear forward operator $\boldsymbol{L}_{viscous}$ can be computed as

$$\boldsymbol{L}_{viscous}\vec{u} = \frac{d}{dx}\left(h\,\frac{\partial\vec{F}}{\partial\vec{U}}\,\vec{u}\right) + \frac{d}{dx}\left(h\frac{d}{dx}\left(\frac{\partial\vec{F}_{v,1}}{\partial\vec{U}}\,\vec{u}\right)\right) + \frac{dh}{dx}\frac{d}{dx}\left(\frac{\partial\vec{F}_{v,2}}{\partial\vec{U}}\,\vec{u}\right) - \frac{dh}{dx}\frac{\partial\vec{P}}{\partial\vec{U}}\,\vec{u}. \tag{7}$$

Using this viscous forward linear operator, and similar to Giles & Pierce (2001), homogeneous forward solutions $\vec{u}(x,\xi)$ are found that satisfy

$$\int_D \boldsymbol{L}_{viscous}\vec{u}_j(x,\xi)d\xi = \int_D \delta(x-\xi)\,\vec{f}_j(\xi)d\xi, \tag{8}$$

by considering solutions of the following form

$$\begin{aligned}\vec{u}(x,\xi) &= a\,H(x-\xi)\,\left(\frac{1}{h(x)}\frac{\partial\vec{U}}{\partial m}\bigg|_{H,q} + c_m(x,\xi)\,\frac{\partial\vec{U}}{\partial q}\bigg|_{m,H}\right) \\ &+ b\,H(x-\xi)\,\left(\frac{\partial\vec{U}}{\partial H}\bigg|_{m,q} + c_H(x,\xi)\,\frac{\partial\vec{U}}{\partial q}\bigg|_{m,H}\right) \\ &+ c\,H(-(x-\xi))\,\left(\frac{1}{h(x)}\frac{\partial\vec{U}}{\partial m}\bigg|_{H,q} + c_q(x,\xi)\,\frac{\partial\vec{U}}{\partial q}\bigg|_{m,H}\right),\end{aligned} \tag{9}$$

where a and b represent uniform perturbations since the nonlinear quasi-1d equations ensure that mass flux and stagnation enthalpy (when $Pr = 3/4$) remain constant along the CD nozzle. The variable c is a uniform amplitude term and the functions $c_{m,H,q}(x,\xi), c_H(x,\xi)$ represent the non-uniform velocity field perturbations that ensure that $\boldsymbol{L}_{viscous}\vec{u}(x,\xi) = \vec{0}$, by satisfying the following homogeneity equations

$$\begin{aligned}&\boldsymbol{L}_{viscous}\left\{a\,H(x-\xi)\,\left(\frac{1}{h(x)}\frac{\partial\vec{U}}{\partial m}\bigg|_{H,q} + c_m(x,\xi)\,\frac{\partial\vec{U}}{\partial q}\bigg|_{m,H}\right)\right\} \\ &= \boldsymbol{L}_{viscous}\vec{u}_1(x,\xi) = \vec{0},\end{aligned} \tag{10}$$

and similarly that $\boldsymbol{L}_{viscous}\vec{u}_2(x,\xi) = \vec{0}$ and $\boldsymbol{L}_{viscous}\vec{u}_3(x,\xi) = \vec{0}$.

Viscous linear adjoint equations and operator: The adjoint equations and operator can be derived by considering the augmented nonlinear objective function (J), where the adjoint solution $\vec{v}$ enforces the differential flow constraints,

$$J = \int_D p\,dx - \int_D \vec{v}^T \cdot \vec{R}\,dx. \tag{11}$$

Linearizing this with respect to perturbations in the flow solution $\vec{u}$ gives $dJ = I$ as

$$I = \int_D \left\{\vec{v}^T \cdot \vec{f} - \left(\vec{v}^T \cdot (\boldsymbol{L}_{viscous}\,\vec{u}) - \left(\frac{\partial p}{\partial\vec{U}}\right)^T \cdot \vec{u}\right)\right\} dx. \tag{12}$$

Integration by parts is used to transfer the differential operator

$\boldsymbol{L}_{viscous}$ from $\vec{u}$ to the variable $\vec{\nu}$ as shown below

$$
\begin{aligned}
I = \int_D \vec{\nu}^T \cdot \vec{f}\, dx - \Bigg[\vec{\nu}^T \cdot (h\boldsymbol{A}\,\vec{u}) - \vec{\nu}^T \cdot \left(h \frac{d}{dx} (\boldsymbol{C}_1\, \vec{u}) \right) \\
+ \frac{d\vec{\nu}^T}{dx} \cdot (h\, \boldsymbol{C}_1\, \vec{u}) - \left(\frac{dh}{dx}\vec{\nu} \right)^T \cdot (\boldsymbol{C}_2\, \vec{u}) \Bigg]_{x=x_{inlet}}^{x=x_{outlet}} \\
- \int_D \vec{u}^T \cdot \Bigg(- h\boldsymbol{A}^T \frac{d\vec{\nu}}{dx} + \boldsymbol{C}_1^T \frac{d}{dx}\left(h\, \frac{d\vec{\nu}}{dx} \right) - \boldsymbol{C}_2^T\, \frac{d}{dx}\left(\frac{dh}{dx}\vec{\nu} \right) \\
- \frac{dh}{dx}\, \boldsymbol{B}^T \vec{\nu}\, - \frac{\partial p}{\partial \vec{U}} \Bigg)\, dx. \quad (13)
\end{aligned}
$$

Therefore the viscous adjoint equation (and adjoint operator $\boldsymbol{L}^{\dagger}_{viscous}$) is (with $\vec{g} = \partial p / \partial \vec{U}$),

$$
\begin{aligned}
\boldsymbol{L}^{\dagger}_{viscous}\vec{\nu} - \vec{g} = - h\boldsymbol{A}^T \frac{d\vec{\nu}}{dx} + \boldsymbol{C}_1^T \frac{d}{dx}\left(h\, \frac{d\vec{\nu}}{dx} \right) \\
- \boldsymbol{C}_2^T\, \frac{d}{dx}\left(\frac{dh}{dx}\vec{\nu} \right) - \frac{dh}{dx}\boldsymbol{B}^T \vec{\nu} - \frac{\partial p}{\partial \vec{U}}. \quad (14)
\end{aligned}
$$

Viscous adjoint solutions $\vec{\nu}(x)$ corresponding to the gradient $\vec{g}(x)$: The adjoint basis solutions can be computed by starting with equation (12), which represents the linearized objective function, the impulse forcing ($\vec{f}(\xi)$) such that

$$
\boldsymbol{L}_{viscous}\, \vec{u}(x,\xi) = \vec{f}(\xi)\delta(x-\xi), \quad (15)
$$

and

$$
\begin{aligned}
I(\xi) = \int_D \vec{g}^T \cdot \vec{u}(x,\xi)\, dx \\
- \int_D \vec{\nu}^T \cdot \Big(\boldsymbol{L}_{viscous}\, \vec{u}(x,\xi) - \vec{f}(\xi)\delta(x-\xi) \Big) dx. \quad (16)
\end{aligned}
$$

Next, equation (16) can be transformed to a form similar to (13) as shown below, using an integration by parts procedure, preserving the terms $\vec{u}(x,\xi)$ or $\vec{f}(\xi)\delta(x-\xi)$ throughout assuming $\boldsymbol{L}^{\dagger}\vec{\nu} - \vec{g} = \vec{0}$ and that these solutions satisfy the adjoint boundary conditions, then together with equation (15) we have

$$
\begin{aligned}
I(\xi) &= \int_D \vec{\nu}^T(x) \cdot \{ \boldsymbol{L}_{viscous}\, \vec{u}(x,\xi) \}\, dx, \quad (17) \\
&= \Bigg\{ \vec{\nu}^T(x) \cdot (h(x)\, \boldsymbol{A}\, \hat{u}_1(x)) \\
&\quad + \vec{\nu}^T(x) \cdot \left(h(x)\, \frac{d}{dx} (\boldsymbol{C}_1\, \hat{u}_1(x)) \right) \\
&\quad + \vec{\nu}^T(x) \cdot \left(\frac{dh(x)}{dx}\, \boldsymbol{C}_2\, \hat{u}_1(x) \right) \\
&\quad - \frac{d\vec{\nu}^T(x)}{dx} \cdot (h(x)\, \boldsymbol{C}_1\, \hat{u}_1(x)) \Bigg\} \Bigg|_{x=\xi}, \quad (18)
\end{aligned}
$$

where the solution $\vec{u}(x,\xi)$ is assumed to have the form $H(x-\xi)\hat{u}_1(x) + \hat{u}_2(x)$ and both $\hat{u}_{i=1,2}$ are homogeneous solutions that satisfy $\boldsymbol{L}_{viscous}\hat{u}_i = \vec{0}$. Furthermore, assuming that the boundary conditions are satisfied for all ξ (on account of the properly constructed solutions $\vec{u}(x,\xi)$), we have the equation

$$
\begin{aligned}
I(\xi) = \vec{\nu}^T(\xi) \cdot \Bigg(h(\xi)\, \boldsymbol{A}\, \hat{u}_1(\xi) + h(\xi)\, \frac{d}{d\xi}\Big(\boldsymbol{C}_1\, \hat{u}_1(\xi) \Big), \\
+ \frac{dh(\xi)}{d\xi}\, \boldsymbol{C}_2\, \hat{u}_1(\xi) \Bigg) - \frac{d\vec{\nu}^T(\xi)}{d\xi} \cdot \Big(h(\xi)\, \boldsymbol{C}_1\, \hat{u}_1(\xi) \Big) \\
(19)
\end{aligned}
$$

which can be solved to obtain the viscous adjoint solutions $\vec{\nu}(\xi)$ corresponding to a gradient $\vec{g}(\xi)$.

Viscous adjoint Green's function operator $\boldsymbol{G}^{\dagger}_{viscous}(x,\eta)$: Starting with equation (19) from the previous section we can now show that

$$
\begin{aligned}
\vec{g}_i^T(\eta) \cdot \vec{u}(\eta,x) = \vec{\nu}_i^T(x,\eta) \cdot \Bigg(h(x)\, \boldsymbol{A}\, \hat{u}(x) \\
+ h(x)\, \frac{d}{dx}\Big(\boldsymbol{C}_1\, \hat{u}(x) \Big) + \frac{dh(x)}{dx}\, \boldsymbol{C}_2\, \hat{u}(x) \Bigg) \\
- \frac{\partial \vec{\nu}_i^T(x,\eta)}{\partial x} \cdot (h(x)\, \boldsymbol{C}_1\, \hat{u}(x)). \quad (20)
\end{aligned}
$$

Upon solving the above partial differential equation for $\vec{\nu}_i(x,\eta)$ for a given gradient $\vec{g}_i(\eta)$, the viscous adjoint Green's function operator $\boldsymbol{G}^{\dagger}(x,\eta)$ can be computed as follows, similar to equation (24) in Murthy & Bodony (2023)

$$
\begin{aligned}
\boldsymbol{G}^{\dagger}(x,\eta) = (\vec{\nu}_1(x,\eta) \mid \vec{\nu}_2(x,\eta) \mid \vec{\nu}_3(x,\eta)) \\
\cdot\ (\vec{g}_1(\eta) \mid \vec{g}_2(\eta) \mid \vec{g}_3(\eta))^{-1}. \quad (21)
\end{aligned}
$$

Viscous forward Green's function operator $\boldsymbol{G}_{viscous}(x,\xi)$: Starting with the equation (17) and whilst considering a forward solutions $\tilde{u}_i(x,\xi)$ such that $\boldsymbol{L}_{viscous}\tilde{u}_i(x,\xi) = \vec{f}_i(\xi)\delta(x-\xi)$, we have

$$
\begin{aligned}
\int_D \delta(x-\eta)\vec{g}^T(\eta)\, \cdot\, \tilde{u}_i(x,\xi)dx = \\
\int_D \vec{\nu}_j^T(x,\eta)\, \cdot\, (\boldsymbol{L}_{viscous} \cdot \tilde{u}_i(x,\xi))dx, \quad (22)
\end{aligned}
$$

$$
\begin{aligned}
\Rightarrow \tilde{u}_i(x,\xi) = (\vec{g}_1(x), \vec{g}_2(x), \vec{g}_3(x))^{-T} \\
\cdot\ (\vec{\nu}_1(x,\xi), \vec{\nu}_2(x,\xi), \vec{\nu}_3(x,\xi))^T \cdot \vec{f}_i(\xi). \quad (23)
\end{aligned}
$$

Next, three linearly independent vectors $\vec{f}_i(\xi)$ must be computed. This can be accomplished by considering the basis vectors $\vec{u}_i(x,\xi)$ and evaluating the following equations to compute the corresponding $\vec{f}_i(\xi)$ as shown below

$$
\begin{aligned}
\vec{f}_i(x) = h(x)\, \frac{\partial \vec{F}}{\partial \vec{U}} \vec{u}_i(x) + h(x)\, \frac{d}{dx}\left(\frac{\partial \vec{F}_{v,1}}{\partial \vec{U}} \vec{u}_i(x) \right) \\
+ \frac{d}{dx}\left[h(x)\, \left(\frac{\partial \vec{F}_{v,1}}{\partial \vec{U}} \vec{u}_i(x) \right) \right] + \frac{dh}{dx}\left(\frac{\partial \vec{F}_{v,2}}{\partial \vec{U}} \vec{u}_i(x) \right).
\end{aligned}
$$

The viscous forward Green's function operator can now be constructed as follows

$$
\begin{aligned}
\boldsymbol{G}_{viscous}(x,\xi) = (\tilde{u}_1(x,\xi), \tilde{u}_2(x,\xi), \tilde{u}_3(x,\xi)) \\
\cdot\ (\vec{f}_1(\xi), \vec{f}_2(\xi), \vec{f}_3(\xi))^{-1}. \quad (24)
\end{aligned}
$$

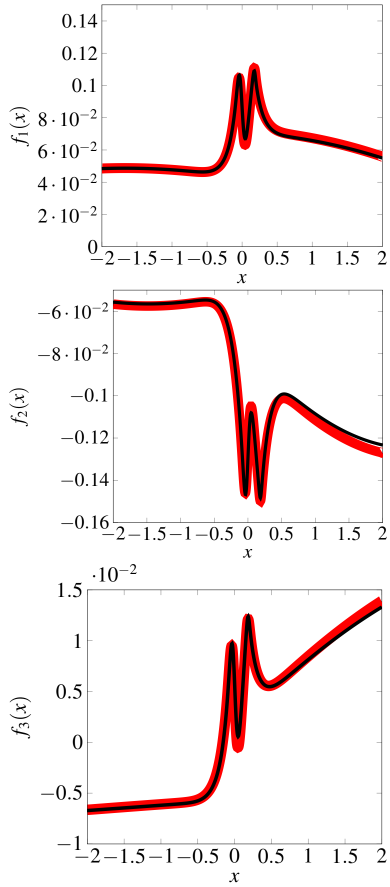

Figure 6. Numerical resolvent forcing mode solution (red) and solution as per the viscous extension of Giles & Pierce (2001) (black), corresponding to the transonic shock-laden flow through a quasi 1d model of flow through a CD nozzle.

Resolvent modes corresponding to viscous shock-laden base-flows: Similar to the inviscid case, the zero-frequency resolvent ($\boldsymbol{R}(\omega=0)$) modes corresponding to the shock-laden flows are computed by solving the eigenvalue problem that originates when computing the SVD of the resolvent operator, given by

$$\boldsymbol{R}^H(\omega=0)\,\boldsymbol{R}(\omega=0)\,\vec{f} = \boldsymbol{G}^{\dagger}_{viscous} * \boldsymbol{G}_{viscous} * \vec{f} = \sigma^2 \vec{f}, \quad (25)$$

here $*$ represents the convolution operation, and the modes computed using $\boldsymbol{R}^H(\omega=0)\,\boldsymbol{R}(\omega=0)\,\vec{f} = \sigma^2 \vec{f}$ and $\boldsymbol{G}^{\dagger}_{viscous} * \boldsymbol{G}_{viscous} * \vec{f} = \sigma^2 \vec{f}$ are in agreement, as shown in Figs. 6 & 7.

RESOLVENT ANALYSIS OF SHOCK-LADEN JETS FROM A BICONICAL NOZZLE

The resolvent modes corresponding to the shock-laden jets from the underexpanded biconical nozzle discussed earlier are now computed with the insight gained from the previous quasi-1d analysis. The base flow, about which the resolvent analysis is performed, is an azimuthally and temporally averaged flow solution of the TTR=1 and NPR = 4 jet described in the LARGE EDDY SIMULATION RESULTS section above. The resolvent modes are computed by a differential version of our WENO-SYMBO* scheme from above produce resolvent modes as shown in figures 8 and 9. The results suggest a possible avenue for JNR: by actuating near the inner surface of the nozzle as highlighted in figure 8.

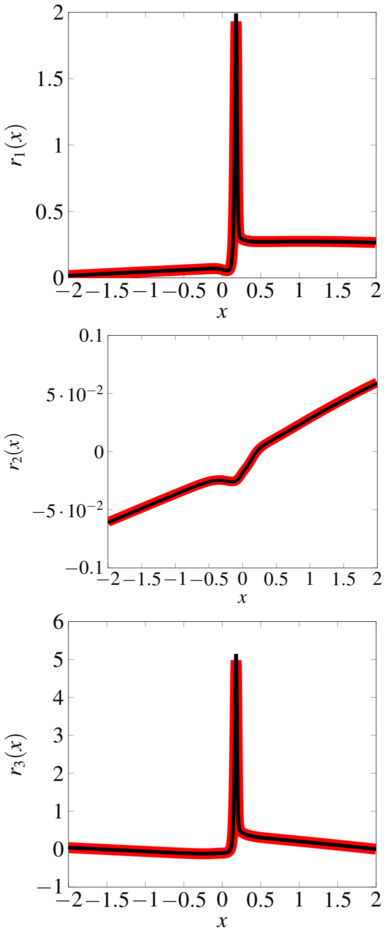

Figure 7. Numerical resolvent response mode solution (red) and solution as per the viscous extension of Giles & Pierce (2001) (black), corresponding to the transonic shock-laden flow through a quasi 1d model of flow through a CD nozzle.

CONCLUSION

The reduction of jet noise is a long sought-after goal and significant progress for subsonic jet JNR has been made through a wavepacket–resolvent approach. When applied to supersonic jets, the presence of shocks at under- or overexpanded conditions introduces discontinuities in the flow and numerical method requirements that may corrupt a linearized analysis. In this paper, motivated by the analysis presented in Bodony & Fikl (2022), we utilized the inviscid Burgers' and Euler equations as shock-laden jet surrogates to determine (a) suitable numerical methods whose linearization yields meaningful forward and adjoint sensitivities (and, consequently, meaningful resolvents) and (b) develop semi-analytical results suitable to verify such methods. Using the quasi-one-dimensional Euler equations, we developed a semi-analytical theory to verify these claims and preliminary results were presented. Future work will focus on producing converging resolvent modes for the Navy relevant shock-laden jet flows and investigate the nature of the singular values of viscous and inviscid shock-laden quasi-1d flows.

ACKNOWLEDGMENTS

This work was sponsored by the Office of Naval Research (ONR), under grant number N00014-19-1-2431. Dr. Steve Martens is the program officer. The simulations were supported by the NSF XSEDE program using allocation

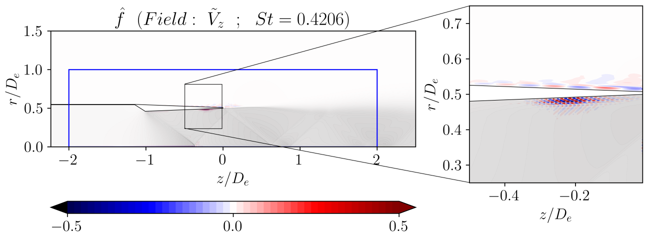

Figure 8. Real forcing mode (color) superimposed on the mean flow (grayscale).

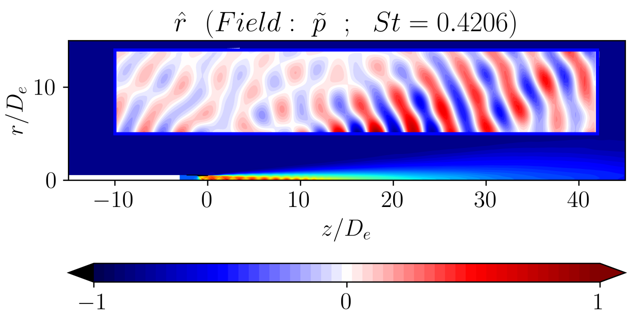

Figure 9. Real response mode, visualized within the box, with the background indicating the mean flow.

CTS20006 & TG-CTS090004 and performed on the TACC Frontera & Stampede2 computers, respectively.

REFERENCES

Beneddine, Samir, Sipp, Denis, Arnault, Anthony, Dandois, Julien & Lesshafft, Lutz 2016 Conditions for validity of mean flow stability analysis. *Journal of Fluid Mechanics* **798**, 485–504.

Bodony, D. J. & Fikl, A. 2022 Adjoint-based sensitivity of shock-laden flows. *Proceedings of the 2022 Summer Program, Center for Turbulence Research* pp. 401–408.

Bridges, James & Brown, Clifford 2004 Parametric testing of chevrons on single flow hot jets. AIAA Paper 2004-2824, Presented at the 10th AIAA/CEAS Aeroacoustics Conference, Manchester, GREAT BRITAIN.

Farrell, Brian F. & Ioannou, Petros J 1993 Stochastic forcing of the linearized navier–stokes equations. *Physics of Fluids A: Fluid Dynamics* **5** (11), 2600–2609.

Farrell, Brian F. & Ioannou, Petros J. 2019 Statistical state dynamics: A new perspective on turbulence in shear flow. *Zonal Jets Phenomenology, Genesis, and Physics.* pp. 380–400.

Garnaud, Xavier, Lesshafft, Lutz, Schmid, PJ & Huerre, Patrick 2013 The preferred mode of incompressible jets: linear frequency response analysis. *Journal of Fluid Mechanics* **716**, 189–202.

Giles, Michael B & Pierce, Niles A 2001 Analytic adjoint solutions for the quasi-one-dimensional euler equations. *Journal of Fluid Mechanics* **426**, 327–345.

Gudmundsson, Kristjan & Colonius, Tim 2011 Instability wave models for the near-field fluctuations of turbulent jets. *Journal of Fluid Mechanics* **689**, 97–128.

Jordan, Peter & Colonius, Tim 2013 Wave packets and turbulent jet noise. *Annual Review of Fluid Mechanics* **45**, 173–195.

Kim, Jeonglae, Bodony, Daniel J & Freund, Jonathan B 2014 Adjoint-based control of loud events in a turbulent jet. *Journal of Fluid Mechanics* **741**, 28–59.

Lesshafft, Lutz, Semeraro, Onofrio, Jaunet, Vincent, Cavalieri, André VG & Jordan, Peter 2019 Resolvent-based modeling of coherent wave packets in a turbulent jet. *Physical Review Fluids* **4** (6), 063901.

Liu, Junhui & Corrigan, Andrew T 2018 Large-eddy simulations of supersonic jet noise generation using wall modeling. In *2018 AIAA/CEAS Aeroacoustics Conference*, p. 3943.

Liu, Junhui, Corrigan, Andrew T, Kailasanath, Kailas, Heeb, Nicholas S, Munday, David E & Gutmark, Ephraim J 2013 Computational study of shock-associated noise characteristics using LES. AIAA Paper 2013-2199, Presented at the 19th AIAA/CEAS Aeroacoustics Conference, Berlin, Germany.

Moin, Parviz, Squires, Kyle, Cabot, W & Lee, Sangsan 1991 A dynamic subgrid-scale model for compressible turbulence and scalar transport. *Physics of Fluids A: Fluid Dynamics* **3** (11), 2746–2757.

Murthy, S. R. & Bodony, D. J. 2023 Resolvent analysis based jet-noise-reduction of a biconical tactical jet nozzle. AIAA Paper 2023-4518, Presented at the 2023 AIAA Aviation Forum.

Norum, TD & Seiner, JM 1982 Broadband shock noise from supersonic jets. *AIAA Journal* **20** (1), 68–73.

Ponton, MK & Seiner, JM 1992 The effects of nozzle exit lip thickness on plume resonance. *Journal of Sound and Vibration* **154** (3), 531–549.

Schmid, Peter J 2007 Nonmodal stability theory. *Annual Review of Fluid Mechanics* **39**, 129–162.

Seiner, John, Ukeiley, Lawrence, Jansen, Bernard, Kannepalli, Chandrashekar & Dash, Sanford 2004 Noise reduction technology for F/A-18 E/F aircraft. AIAA Paper 2004-2972, Presented at the 10th AIAA/CEAS Aeroacoustics Conference, Manchester, GREAT BRITAIN.

Sipp, Denis & Marquet, Olivier 2013 Characterization of noise amplifiers with global singular modes: the case of the leading-edge flat-plate boundary layer. *Theoretical and Computational Fluid Dynamics* **27** (5), 617–635.

Williams, JE Ffowcs & Maidanik, G 1965 The mach wave field radiated by supersonic turbulent shear flows. *Journal of Fluid Mechanics* **21** (4), 641–657.